Changing the chemical composition of dissimilar Mg/Al friction stir welded butt joints by addition of zinc interlayer

A. Abdollahzadeh[1, 2], A. Shokuhfar[1], J.M. Cabrera[2], A.P. Zhilyaev[2, 3], H. Omidvar[4]

[1] Faculty of Materials Science and Engineering, K. N. Toosi University of Technology, Tehran, Iran.
[2] Department of Materials Science and Metallurgical Engineering, Polytechnic University of Catalonia, Barcelona, Spain.
[3] Institute for Problems of Metals Superplasticity, Russian Academy of Sciences, Ufa, Russia.
[4] Faculty of Mining and Metallurgical Engineering, Amirkabir University of Technology, Tehran, Iran.

Abstract

In this study, solid state joining technology of friction stir welding (FSW) was carried out for Al and Mg butt joints. To improve the microstructural characteristics of the banded structure zone, before to the FSW process, a Zn interlayer was also inserted in the butt joints. Optimal conditions for friction stir welding were obtained using a combination of two travel speeds (25 and 35 mm/min) and three rotation speeds (550, 600 and 650 rpm). Mg-Zn and Mg-Al-Zn IMCs, Al solid solution and residual Zn were the most common phases in the stirred zone, eliminating Al-Mg intermetallic formation. The joint fabricated at 35 mm/min and 600 rpm, in which tensile strength of the weld improved from 141 to 175 MPa and an elongation from 0.7 to 1.9 was achieved, gave the maximum mechanical properties compared with the Zn free sample FSWed under identical conditions. The fracture micrographs were compatible with the corresponding ductility results and the fracture surfaces of Zn added samples possessed a fine texture combining brittle and ductile fracture features. Meanwhile, the hardness level was lower than that of the Zn free sample because of the change in the IMCs composition of the Zn added samples.

Keywords: Dissimilar FSW, Zn Interlayer, Al/Mg butt joint, Intermetallics, Microstructure, Mechanical properties.

1. Introduction

Aluminum alloys have been extensively applied in different industries such as electronics, aerospace, shipbuilding and automotive, given their outstanding characteristics, namely good formability, high strength, good corrosion resistance and low weight [1,2]. Mg alloys have been used in electronic and transportation industries since they are the lightest among structural metals and they have high specific strength and rigidity and good damping capacities [3,4]. A major benefit for the production of light weight structures, energy saving and reduction of emission is the successful aluminum and magnesium dissimilar welding [5,6]. The high temperature in the fusion welding between Mg and Al alloys forms a large number of brittle Mg-Al intermetallic compounds (IMCs). This is more disastrous on the Al-Mg interface [7]. In addition, most of these dissimilar welds have drawbacks such as large heat affected zone (HAZ), porosities, solidification cracking, losses because of evaporation and high residual stresses [8]. The

development of a perfect joining process between these metals is a decisive requirement to achieve a good combination of the characteristics of Mg and Al alloys. Therefore, solid state methods, as an alternative technology for joining Al and Mg, are of great interest [9,10].

The Welding Institute of the UK developed friction stir welding as a solid state joining technology in 1991. In this process a rotating tool formed by a shoulder and a pin is placed at a fixed rate inside a joint between two fastened parts of the material. Sufficient heat is generated by the friction between the material and the shoulder to plastify the joint and a powerful bond between the materials is promoted by the pin stirring. Unlike other welding processes, this technique is characterized by the absence of melting, low temperature and low heat input [11,12]. These properties give rise to the wide application of FSW in dissimilar welding [13–17]. Much work has been carried out on the FSW of Al to Mg in butt and lap joints [18–21]. The presence of mass brittle IMCs such as $Al_{12}Mg_{17}$ and Al_3Mn_2 may not be ignored in spite of successful FSW of Al-Mg and preventing the thick interlayer of brittle IMCs [22–25]. Brittle fracture is caused by these IMCs.

The impact of interlayer or addition of alloying element on the reduction or elimination of Al-Mg-IMCs formation and the microstructure and mechanical properties of Al/Mg have recently been investigated [26–30]. At low temperatures, Zn preferably reacts with Mg to yield Mg-Zn IMCs, based on the phase diagrams of Mg-Zn and Al-Zn. Furthermore, a large solid solubility may be formed between Zn and Al, which causes Zn to function as an alloying element and improves the mechanical characteristics of the FSW Mg-Al joint [31,32]. According to the previous literature reports, the significant part of Zn interlayer in joining Al and Mg alloys is obvious since Zn can prevent the excessive reaction between Al and Mg atoms. This phenomenon inhibits Mg-Al and Mg-Zn binary IMC formation. improving therefore the mechanical properties of the joints [32–35].

In most of the published works, fusion welding methods have been used in order to join the dissimilar lap joints. In the case of lap joint, this is usually associated with the formation of a transition layer of the interlayer material as a barrier between the two base metals. However, to the best of the authors' knowledge, the application of Zn interlayer in butt joints of 6061 Al alloy and AZ31 Mg alloy made by FSW as a solid state joining technology has not yet been reported.

Thus, the objective of this work is the investigation of the potential of using Zn interlayer in dissimilar FSW butt joint of 6061 aluminum alloy to AZ31 magnesium alloy. The effects of rotational and traveling speeds on macrostructure, microstructure and mechanical behavior (tensile tests and hardness) of the Zn added joints have been investigated to gain a perfect joint. An optimized joint free of Zn interlayer has also been prepared and tested for comparison purposes.

2. Experimental investigation

2.1. Materials and methods

In this work, 5 mm thick sheets of AZ31 Mg and 6061-T6 Al alloys were cut into samples of 60 mm width and 100 mm length. The nominal chemical contents and mechanical characteristics of both alloys are shown in Table 1.

Table 1
Chemical contents and mechanical characteristics of alloys.

alloys	Chemical contents (weight percent)									Mechanical characteristics		
	Al	Mg	Si	Zn	Fe	Cu	Mn	Cr	Ti	Ultimate strength (MPa)	Elongation (%)	Hardness (HV)
Al 6061	Bal.	0.9	0.64	0.003	0.3	0.25	0.01	0.1	0.02	320	14	105
Mg AZ31	2.84	Bal.	-	1.17	0.004	-	0.15	-	-	255	12	55

Following grinding, 0.3 mm thick Zn interlayers were fixed between aluminum and magnesium strips and plates butt welded at a combination of three rotational (550, 600 and 650 rpm) and two traveling speeds (25 and 35 mm/min) using a purpose built fixture. The best mechanical characteristics were obtained in samples welded at travel and rotation speeds of 35 mm/min and 600 rpm, respectively. Consequently, friction stir welding was also carried out using the same process parameters, but without applying Zn interlayer to comprehend the influences of Zn interlayer on the microstructural and mechanical characteristics of the welds. Fig. 1 shows a simple schematic representation of the applied dissimilar FSW process with addition of Zn interlayer. Table 2 lists the process parameters employed in this work. In addition, the data associated with samples and processing conditions are summarized in Table 3. Friction stir welding tool was fabricated using H13 steel at a hardness of 50 HRC. Table 4 provides the tool details.

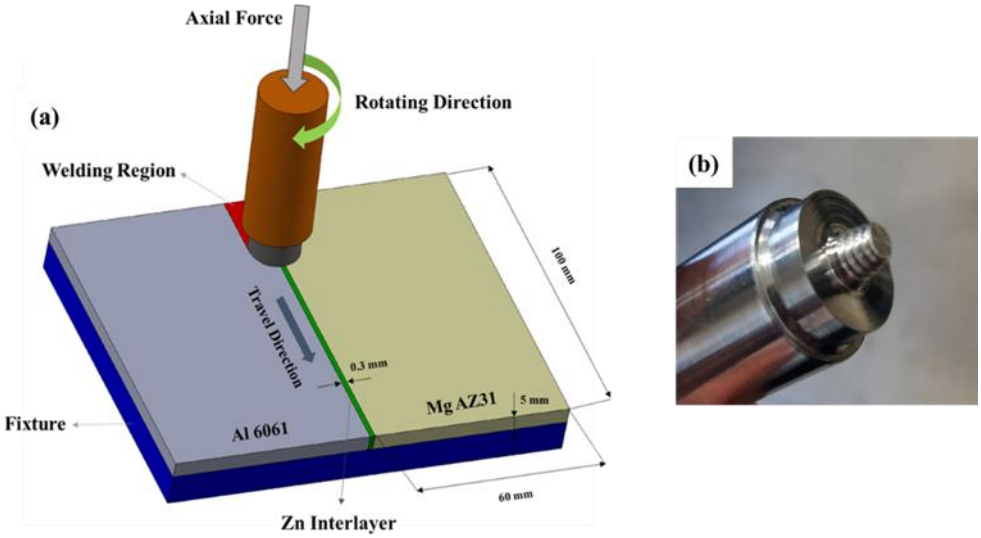

Fig. 1. (a) A schematic picture of FSW process with addition of Zn interlayer, (b) FSW tool.

Table 2
Parameters of friction stir welding process.

Process	Rotational Speed (rpm)	Traveling speed (mm/min)	Tilt angle (degree)	Position	Offset	Number of pass
FSW	550 - 600 - 650	25 - 35	3	Mg (advancing side)/ Al (retreating side)	1 mm toward Mg	1 pass

Table 3
Identification and process conditions of samples.

Sample identification	1	2	3	4	5	6	7
Rotational speed (rpm)	550	550	600	600	650	650	600
Traveling speed (mm/min)	25	35	25	35	25	35	35
Condition	With Zn interlayer	With Zn interlayer	With Zn interlayer	With Zn interlayer	With Zn interlayer	With Zn interlayer	Without Zn interlayer

Table 4
Detailed features of the tool used for friction stir welding process.

Process	Tool material	Shoulder diameter (mm)	Surface of shoulder	Shape of pin	Big diameter of pin (mm)	Small diameter of pin (mm)	Length of pin (mm)
FSW	H13 Steel	15	Concave	Frustum	6	4	4.8

2.2. Microstructural characterization

Cross sectional samples were cut vertical to the FSW direction to perform metallographic experiments. The microstructural preparation was carried out based on ASTM-E3. Joints were first mechanically polished up to 4000 grit, followed by polishing using an Al_2O_3 solution of up to 1 µm powder size.

Optical microscopy (Olympus GX51), field emission scanning electron microscopy (FESEM-JEOL JSM-7001F operated at 20 kV) and high resolution transmission electron microscopy (Philips C2100 at an accelerating voltage of 200 kV) were used to invetigate both the macrostructure and microstructure.

Transmission electron microscopy (TEM) samples were prepared by conventional mechanical polishing. Samples were first cut and then ground to a thickness below 100 µm using 1000 grit abrasive paper. Subsequently, a 3 mm disc was punched out from the sample. The region containing IMCs next to the advancing side, which consisted of the Mg/Al interface, was selected as the punch area based on the optical micrograph. The punched samples were then polished using diamond paste and ion milling was finally applied for thinning.

2.3. Mechanical characterization

Tensile samples in sub-sized scale were prepared vertical to the FSW direction based on ASTM-E8. A universal testing machine INSTRON-5502 was used to carry out tensile tests at room temperature and at a strain rate of 0.5 mm/min. An FEI Quanta 200 SEM equipment and X-ray diffraction (XRD) patterns were used to study the fracture surface. Microhardness tests were performed across the middle of metallographic samples. A Micro Vickers hardness tester (Buehler Micromet 2) with 25 g load and 10 s holding time was used for this purpose. Each indentation point was 0.5 mm away from the other ones.

3. Results and discussion

3.1. Joint appearance and macrostructure

The appearance and macrostructure of Mg/Al friction stir welded joints at different rotational and traveling rates are shown in Fig. 2. Fig. 3 shows the selected regions in larger magnification. In the cases of samples 1 and 2, low rotational speed and insufficient intermixing of materials caused some tunnel defects and cavities on the surface and the bulk of the butt joints. In sample 2, a crack reaching from the bottom to the surface of the sample is visible, indicating the continuity of the tunnel defect along the weld. In addition, incomplete stirring of the material in the weld zone is one of the problems observed in the macrograph of this sample, which was exposed to the lowest temperature during FSW process (minimum rotational speed and maximum traveling speed).

Different plastic flows occur between Al and Mg under low heat input conditions. According to the observed tunnel and cavity formation, there may be a discontinuity in the material flow. It must be pointed out that low heat input limits the formation of IMCs in the stirring zone, but this is not the case here [24].

The formation of a small tunnel defect on the joint surface and the presence of some micro cavities inside the weld zone of sample 5 are visible (see Figs. 3(c) and 3(d)). During FSW process (maximum rotational speed and minimum traveling speed), this sample was subjected to the highest temperature. A good plastic flow in the stirring zone (SZ) is provided by these conditions. However, a large number of flashes tend to form on the weld surface as the heat input increases. Therefore, defects including tunnel and cavity on the advancing side appear because of the metal loss.

Defects such as tunnels, cracks and voids are not observed in other samples whereas the weld surface shows smooth semi-circular traces. In addition, a more homogenous intermixing of Mg and Al alloys and appropriate flow pattern are obtained in the stir zone of these samples resulting from the good penetration of Al and Mg into each other (see macrostructures).

As Mishra et al. [36] reported, the low heat generation in the welding zone can be not enough to soften the materials and cause a bad stirring in the SZ. Voids or other defects may be observed inside the stirred zone in a cold material. Under some severe conditions, the tool can even break due to the high forces involved. Moreover, given the extreme formation of flash, the presence of phases with low melting points (constitutional liquation) and the chance to grain growth, the extra heat input condition may damage the final properties of the joint.

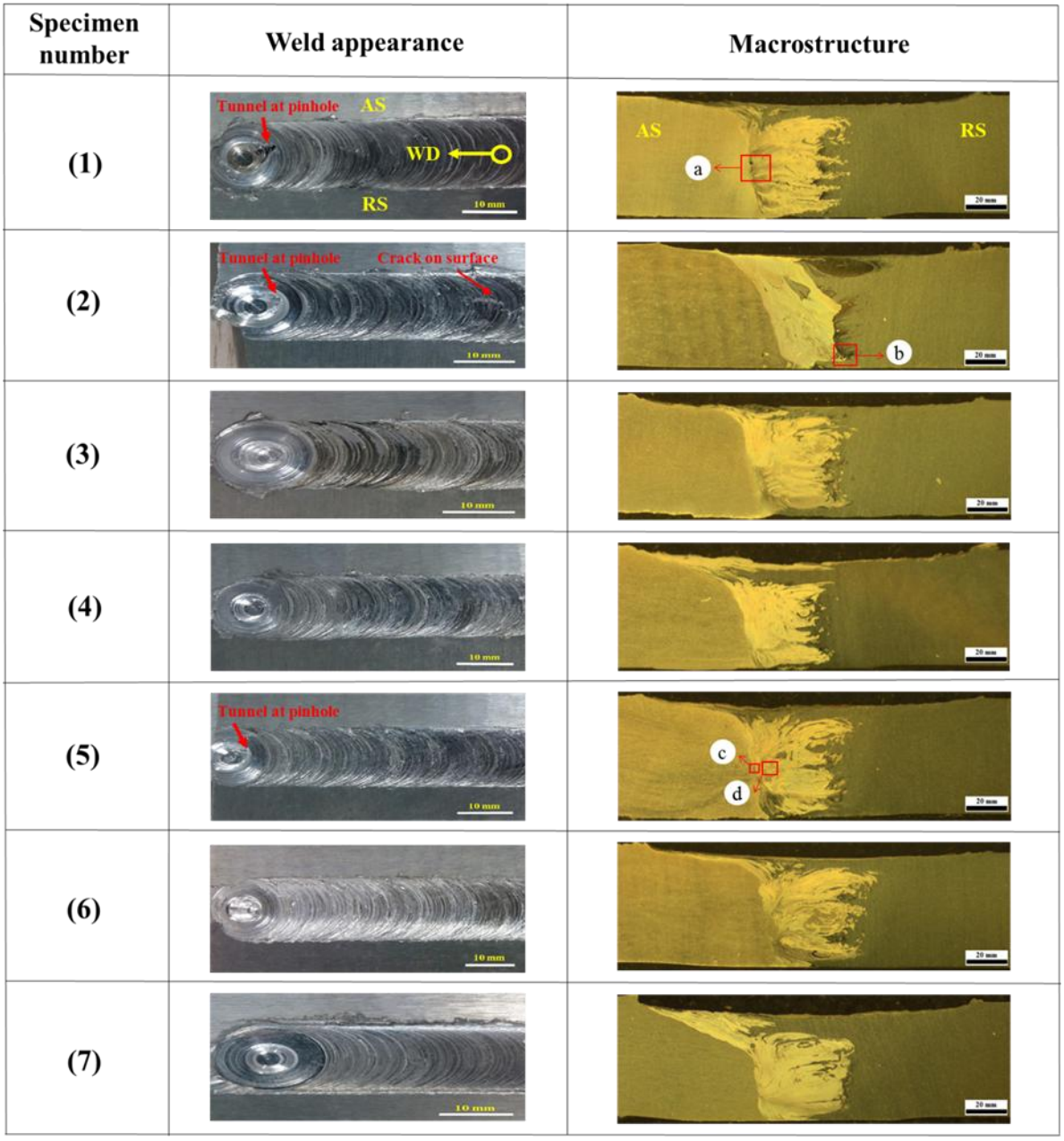

Fig. 2. Joints appearance and macrostructure of different samples welded using various welding conditions, namely rotational and transversal speeds. Processing conditions of each sample are listed in Table 3.

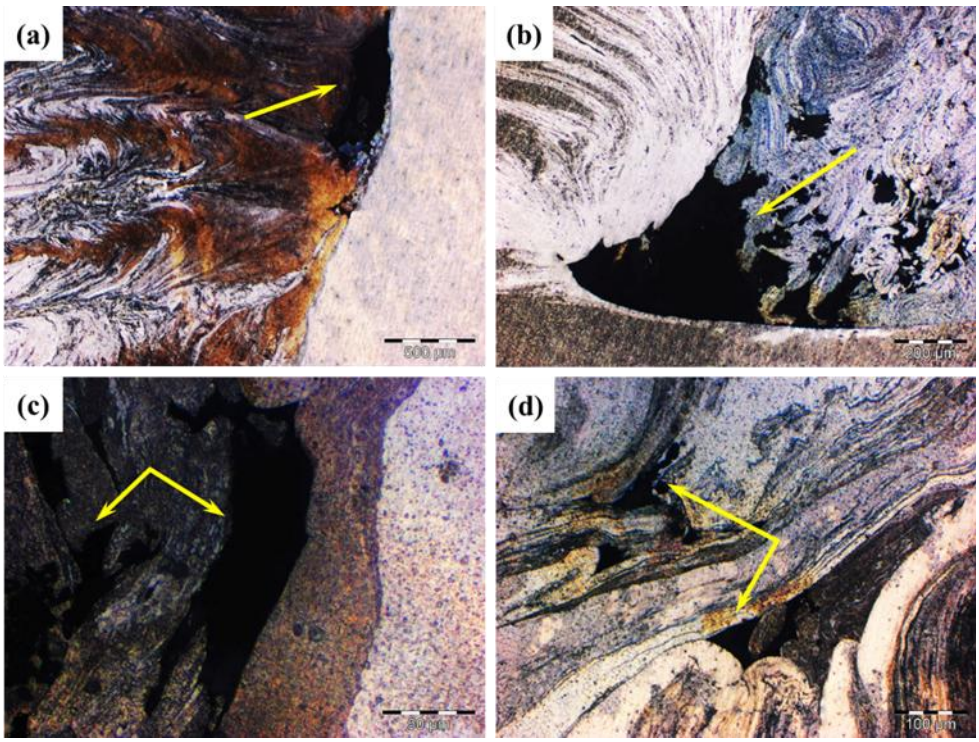

Fig. 3. Enlarged graph of areas pointed in Fig 2 show presence of cavity in the stirred zone of: (a) sample 1, (b) sample 2, (c,d) sample 5.

Fig. 4(a) shows the detailed macrostructure analysis of sample 4. Two distinct zones are observed: (1) a banded structure (BS) zone and (2) a severely deformed zone (SDZ) in the middle of the weld nugget [22].

A part of the advancing side of the joint is shown in Fig. 4(b). The Zn poor and rich regions (in white color) can be observed. Fig. 4(c) shows the Zn rich region at higher magnification. Formation of some thin intermetallic layers is visible in this graph. Fig. 4(d) shows the Mg alloy interface and the banded structure zone on the Mg side. It must be indicated that the BS zone is accounted for the failures of most Al/Mg welded joints, given the presence of a large number of IMC [22,37].

However, in the present case, no visible alternating bands or continuous layer of intermetallics can be observed near the Mg interface. The region near Mg interface consists of α (Mg) + Mg-Zn phases, according to the EDS analysis.

The retreating side and severely deformed zone in the nugget zone are shown in Fig. 4(e). The severely deformed zone showed complex and disordered patterns, which are represented by magnesium and aluminum swirls and vortexes, associated with the spiral flow of metals in the FSW process. Similar observations have previously been reported [10,21].

It can be observed that the regions with unreacted Zn (white regions) increase from the advancing to the retreating side. Considering that the heat input and the exposure time of the material to the high temperature on the retreating side are lower than those in the advancing side [38], a greater amount of unreacted Zn element will remain on the RD side.

Figs. 4(f) and 4(g) show the aluminum and nugget zone interface and a higher magnification view of onion rings, respectively, which confirms appropriate plastic flow of material. In addition, IMC formation near the interface of nugget zone and aluminum alloy is shown in Fig. 4(f). The intermetallics near the Al alloy are Al-Mg-Zn compounds, according to the EDS analysis.

The border of nugget zone and adjoining alloys are observed to be sharper and clearer on the magnesium side than in the aluminum side. Zhao et al. [19] reported that the material plastic flow is in the same direction with the welding route on the advancing side of the stirred zone. Therefore, a distinct border is formed between the Mg alloy and the nugget zone. However, the deformation of the base material and the welding route are in opposite directions on the retreating side, causing no clear border between the nugget zone and the Al alloy on this side.

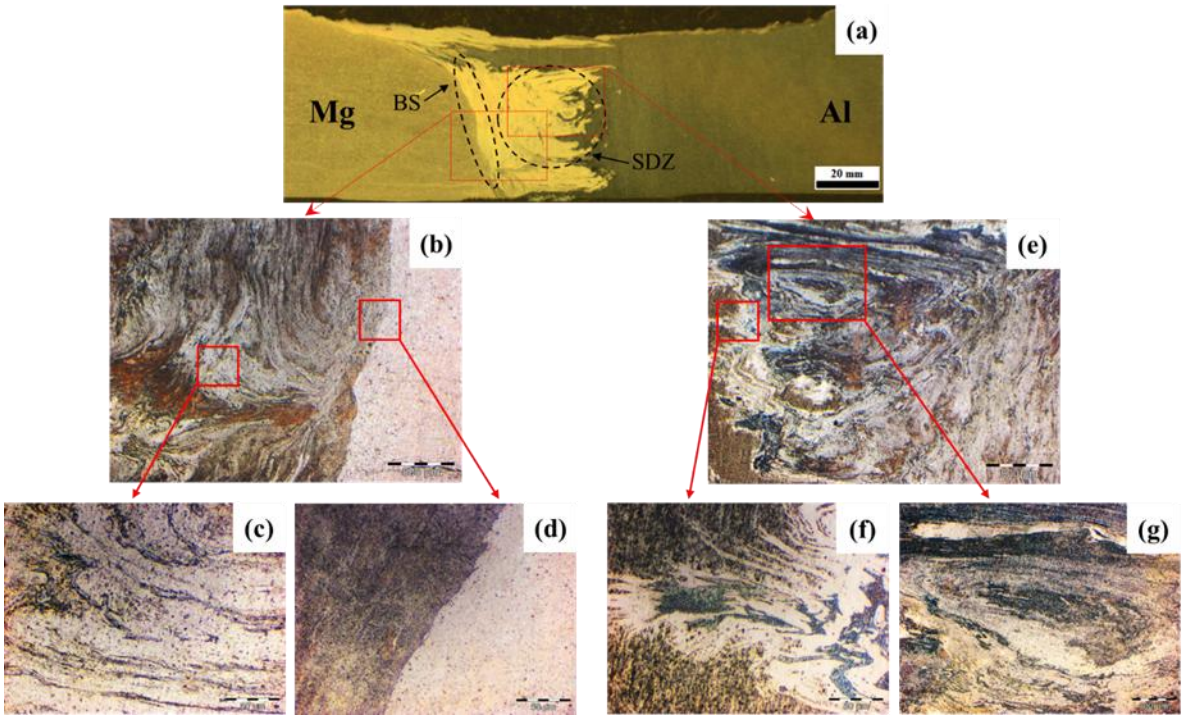

Fig. 4. Optical graphs of specimen 4 (joint welded at 600 rpm and 35 mm/min): (a) Transverse cross-section, (b-d) different regions of advancing side, (e-g) different regions of center and retreating side.

3.2. Microstructural observation

In butt FSWed joints of the Al/Mg alloys, the BS zone near Mg alloy is responsible for most of the failures, as previously indicated. According to the literature reports [22,37], abundant alternate brittle Al-Mg IMCs layers form in the BS zone of the welds, facilitating the propagation of cracks. In addition, the angle between the IMC band direction in the BS and tensile is 45°, pushing the maximum shear stress in this case to the IMC bands. Furthermore, the fracture may initiate from the hot cracks, which are formed in the BS, during solidification.

Fig. 5 shows the banded structure zone for all samples at different rotational and traveling speeds. In order to derive the chemical nature of the IMCs and phases, EDS analysis was carried out at the locations marked as point 1 to 6 (Table 5). FESEM micrographs of samples 1 and 2 with the rotational speed of 550 rpm are presented in Figs. 5(a)

and 5(b), respectively. According to the EDS analysis, in sample 1, layers of Al-Mg intermetallics ($Al_{12}Mg_{17}$) were formed in the BS zone and on the border of Mg alloy. Enough plastic flow of the metal would not occur at low rotation speed if the temperature for melting the Zn interlayer is not high enough. Therefore, the Zn interlayer cannot effectively prevent the formation of the Mg-Al intermetallic bands. For sample 2, as the coldest weld sample, insufficient stirring and incomplete intermixing of materials occur due to the low rotation and high travel speeds, according to the optical observations (Fig. 3(b)). Therefore, although some Zn rich zones are observed near the Mg boundary, there is no clear and normal interface in this sample.

Figs. 5(c) and 5(d) show BS zone FESEM micrographs of samples 3 and 4, welded at 600 rpm rotational speed. In these samples, no visible alternating bands or continuous layer of the Al-Mg IMCs can be observed in the BS zone. The heat input is good enough to make appropriate intermixing of materials and melt a sufficient amount of the Zn interlayer. Moreover, the diffusion of Zn elements to the base materials is easier. Consequently, the formation of Mg-Zn intermetallic compounds prevents the formation of Al-Mg IMCs in the BS zone and interface of the Mg alloy. The presence Zn poor and rich regions (in white color) in the BS zone of sample 3 suggest the non-uniformity of Zn elements in this zone. On the other hand, sample 4 shows a uniform and homogenous structure without the presence of any Al-Mg IMCs bands near the Mg interface. According to the EDS analysis, the region indicated by points 3 consists of both magnesium and zinc, the amount of magnesium being greater. This suggests that the phase is an α (Mg) + $MgZn_2$ eutectic structure and the formation of this structure in Zn added Al/Mg joints is consistent with the reports of Zhang et al. [39] and Gao et al. [34].

Mg-Zn eutectic microstructure is famous for its hardness and brittleness. However, the dispersive distribution of Mg-Zn second phase particles can prevent the crack propagation.

The FESEM micrograph of samples 5 and 6 banded structure zone are presented in Figs. 5(e) and 5(f), respectively. In both samples, continuous Al-Mg IMCs ($Al_{12}Mg_{17}$) bands next to the eutectic structure (α (Mg) + $MgZn_2$) can be observed. These Al-Mg IMC layers for sample 5, which was exposed to the higher temperature, are more catastrophic and thicker. These samples were exposed to the highest temperature (welded at a rotational speed of 650 rpm). In addition, the low Zn melting point resulted in constitutional Zn liquation in the shoulder contact area and squeezing out under the FSW tool action. This verified the fact that the increased heat input and the enhanced plastic metal flow caused the significant deficiency of the Zn element at the interface because of extreme speed rotation. Thus, many Al-Mg IMCs with a typical banding shape have shown up.

Banded structure of sample 7 (same conditions as those for sample 4, but without the addition of Zn interlayer) is also shown in Fig. 5(g), which indicates the catastrophic formation of thick Al-Mg IMC layers (see Table. 5) near the Mg interface.

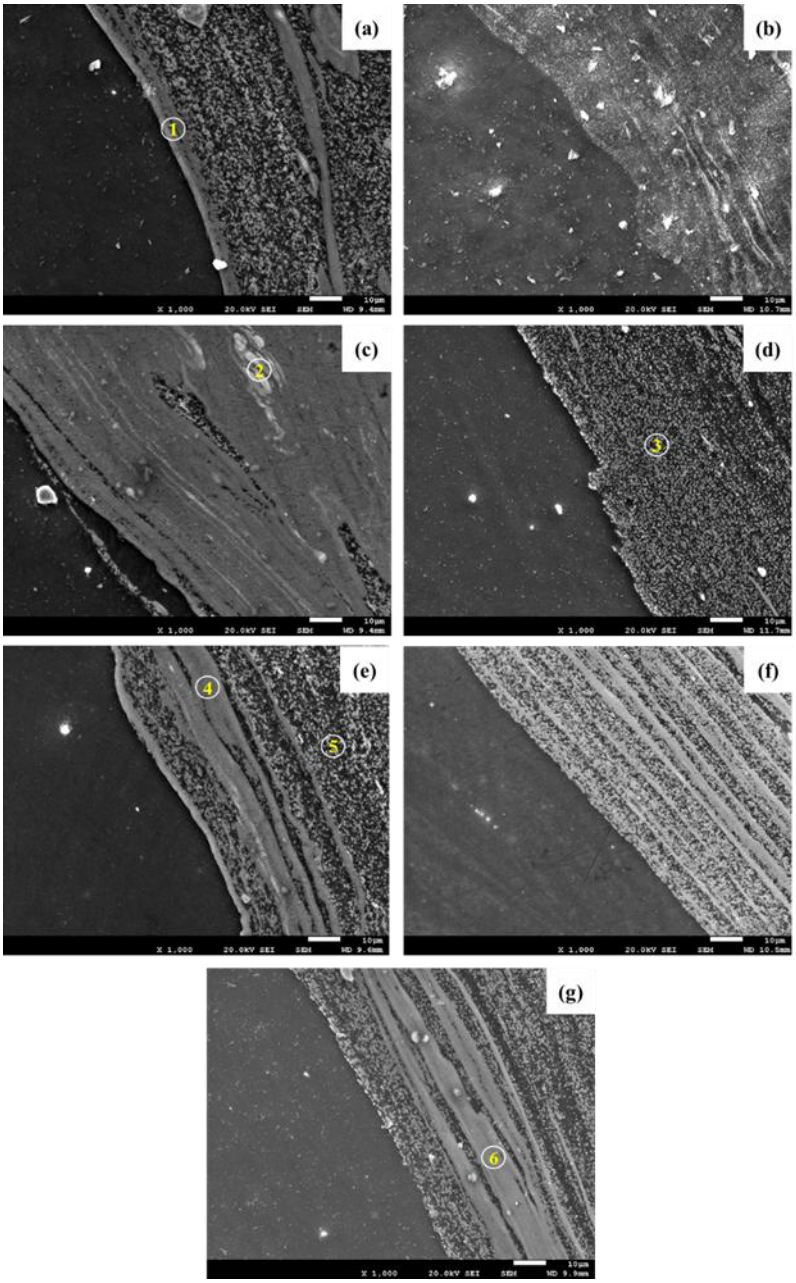

Fig. 5. FESEM micrograph of banded structure zone in specimen: (a) number 1, (b) number 2, (c) number 3, (d) number 4, (e) number 5, (f) number 6, (g) number 7.

Table 5
Compositions (%Weight) determined by EDS at locations demonstrated in Fig. 5.

Location	Mg	Al	Zn	Possible Phase(s)
1	59.18	34.21	5.63	$Al_{12}Mg_{17}$
2	37.16	4.38	57.45	$Zn + MgZn_2$
3	63.26	5.86	30.31	α (Mg) + $MgZn_2$
4	60.56	32.42	6.09	$Al_{12}Mg_{17}$
5	65.53	3.97	29.72	α (Mg) + $MgZn_2$
6	62.78	35.83	0.57	$Al_{12}Mg_{17}$

Fig. 6(a) shows a low magnification of the sample cross sectional view made at 600 rpm and 35 mm/min. SEM analysis was carried out by focusing on the severely deformed zone and borders of magnesium and aluminum alloys with nugget zone, which possessed typical characteristics significantly distinct with similar friction stir welding joints. In order to derive the IMC chemical nature, EDS analysis was carried out at the locations marked as point 1 to 6 (Table 6).

The microstructure and phases of the welded joint are directly associated with the reaction among the Zn interlayer, AZ31 Mg substrate and 6061 Al substrate under the stir tool action during Mg-Al FSW with the Zn interlayer addition. Zn has reacted differently with the Mg and Al substrates in different zones because of the differences in material flow and heat input.

Typical SEM images of the top and bottom interface between Mg and nugget are shown in Figs. 6(b) and 6(c). There is no sign of Al-Mg IMCs layers in the top or bottom of Mg interface. In addition, there are more regions with the residual Zn (white color areas) in the bottom, which were exposed to the lower temperature during FSW process. As indicated in the previous section, according to the EDS analysis (point 3 in Fig. 5), it is suggested that the area near the Mg interface is an α (Mg) + Mg-Zn eutectic phase.

Figs. 6(d) and 6(e) show typical SEM images of the bottom and top interfaces between Al and nugget. EDS analysis from the locations marked in Fig. 6(e) (points 1-3) confirms the presence of α (Mg) + Mg-Zn eutectic structure, Al-Mg-Zn_4 intermetallic compound and Al solid solution in different regions near the Al interface.

Ternary IMCs are mostly $Al_6Mg_{11}Zn_{11}$, which is ordinary under equilibrium cooling conditions, based on the Al-Zn-Mg phase diagram [40]. Nevertheless, there is no $Al_6Mg_{11}Zn_{11}$ in the stirred zone, according to the EDS results. The composition is rather closer to the $Al_5Mg_{11}Zn_4$ previously reported by Zhang et al. [39], who showed that some non-equilibrium state reactions can take place during the solidification process, justifying the presence of $Al_5Mg_{11}Zn_4$.

On the other hand, Al solid solution between IMCs and the matrix materials can play a significant role in transiting stress and making stress concentration and the extension of cracking harder [32,34]. Nevertheless, the regions near

the Mg alloy substrate have less Al solid solution compared with those in the center and near the Al alloy substrate. This may be another explanation for the banded weak structure in the Mg side.

Figs. 6(e-g) show two distinct zones in the top and bottom of the severely deformed zone, respectively. At the top, near the shoulder, which is the main FSW heat source, the greater quantity of Zn filler metal melts and solidifies later than at the bottom of the joint. Therefore, the Zn atoms at the top have more time for diffusion into the stirred zone. This is why the white color regions, which indicate the presence of the unreacted Zn, increase from the top to the bottom of the joint.

Figs. 6(h-i) show the FESEM micrograph and EDX mapping of Zn element distribution in the severely deformed zone, which confirms the appropriate diffusion and presence of Zn elements in this area.

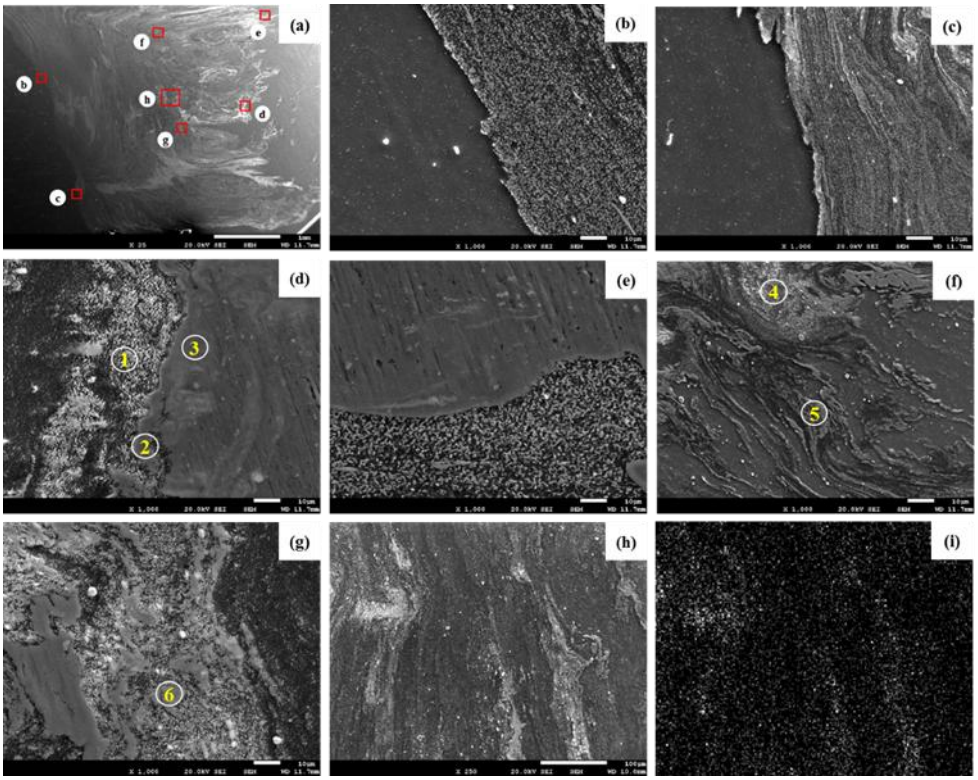

Fig. 6. FESEM micrograph and EDS examination of reinforced sample made at 600 rpm and 35 mm/min: (a) cross-sectional view of joint, (b-h) Enlarged graph of areas pointed in (a), (i) EDX mapping of the areas pointed in (h).

Table 6
Compositions (%Weight) determined by EDS at locations demonstrated in Fig. 6.

Location	Mg	Al	Zn	Possible Phase(s)
1	57.12	7.06	35.15	α (Mg) + MgZn2
2	41.23	32.86	25.48	$Al_5Mg_{11}Zn_4$
3	11.39	58.66	28.83	α (Al) + $MgZn_2$
4	59.95	4.37	34.80	α (Mg) + $MgZn_2$
5	61.02	20.54	17.45	α (Mg) + $Al_5Mg_{11}Zn_4$
6	46.66	28.37	24.51	$Al_5Mg_{11}Zn_4$

The FESEM image and EDS line scan of the distribution of main elements (Al, Mg, and Zn) in the Mg and nugget zone interface are shown in Fig. 7. Mg decreased while Zn increased from Mg alloy toward the nugget zone. In addition, the aluminum number increases slightly. The main regions of the nugget close to Mg alloy contain both Mg and Zn elements, as implied by the elemental distribution results. This suggests the presence of uniform eutectic structure in this area. Furthermore, uniform composition is an advantageous property of the joint.

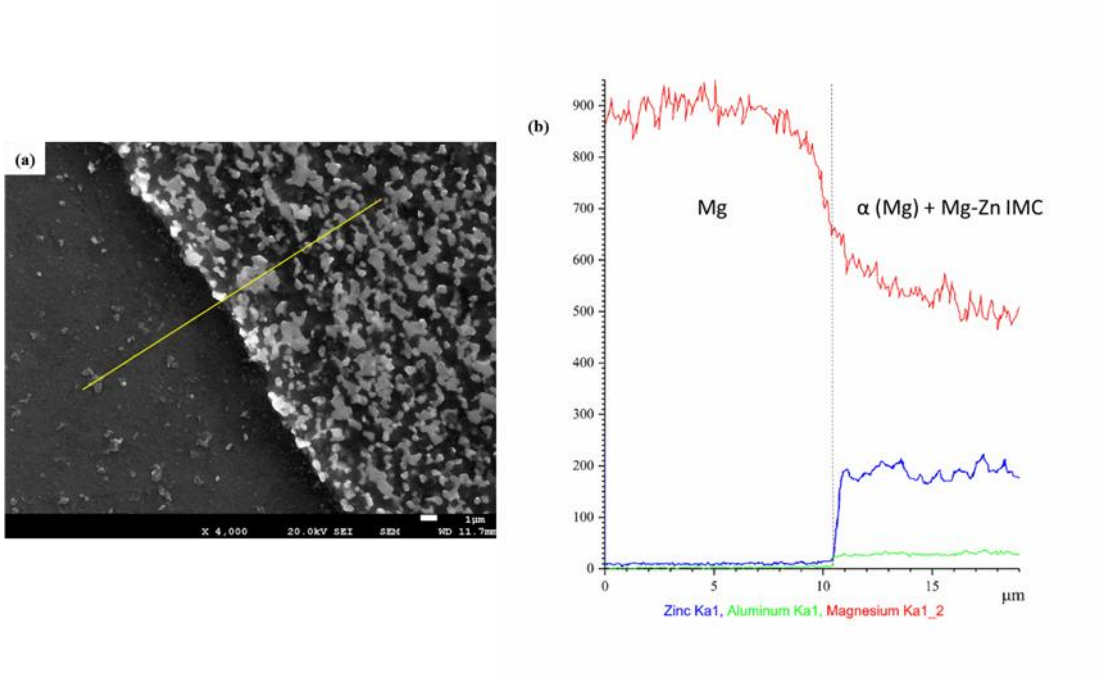

Fig. 7. EDS line analysis at Mg interface of specimen welded at 600 rpm and 35 mm/min.

Fig. 8 display the FESEM image and related SEM-EDS line analysis outcomes for distributions of major elements (Al, Mg, and Zn) in the interface of Al and nugget zone. A remarkable fluctuation in the concentration of elements is noticed near the Al interface in the figure, implying the formation of different phases along the EDS line. Fig. 8(b) shows the suggested phases formed in each region.

Generally, the microstructural observations and EDS analysis in various parts of the weld show that the reaction between Al and Mg atoms has been prevented by the Zn interlayer and Mg-Zn has been replaced by less brittle Al-Mg-Zn IMCs. The Mg and Zn standard molar enthalpy is much smaller than that of Al and Mg [31,32]. Moreover, Zn and Mg possess identical crystal lattice. Consequently, Mg-Zn IMCs may precipitate prior to Mg-Al brittle IMCs and Mg and Zn elements are the main components at the joint interface and extremely deformed zone, which agrees well with the previously reported data [33,35].

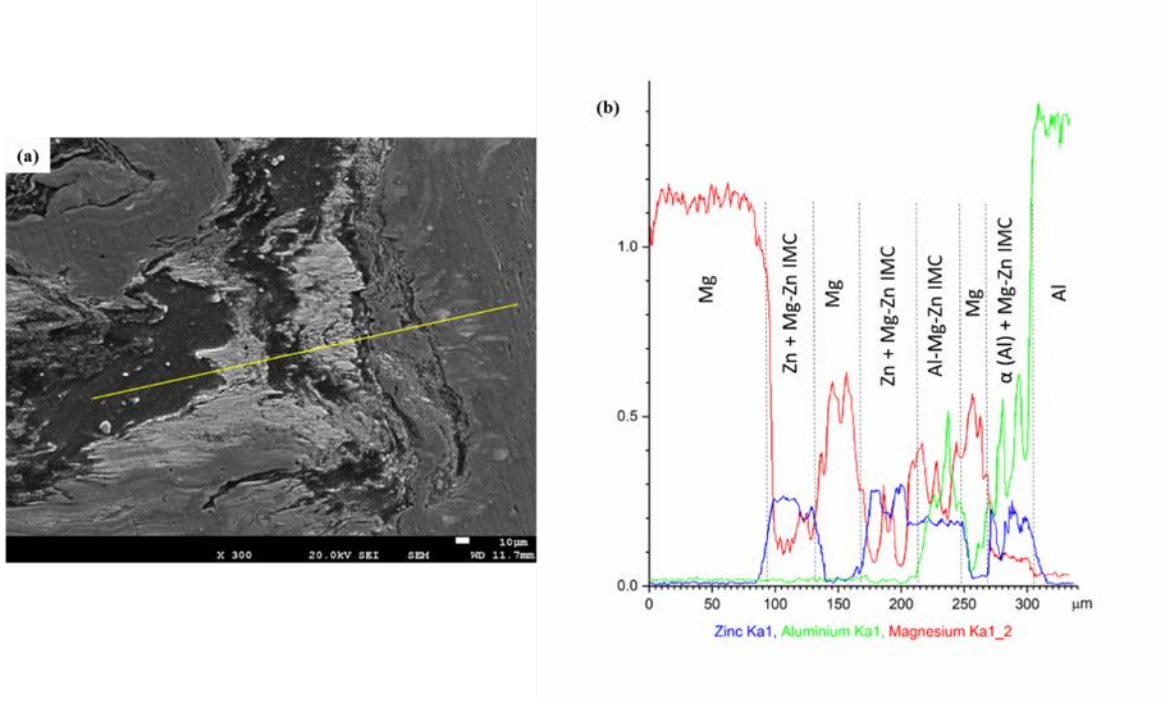

Fig. 8. EDS line analysis at Al interface of specimen welded at 600 rpm and 35 mm/min.

TEM images from a region of stirred zone near the Mg interface in sample 4 are shown in Figs. 9(a-b). The presence of residual Zn in the rippled area of Mg matrix is confirmed by EDS peaks obtained from location c (Fig. 9(c)). However, the presence of Mg-Zn IMC ($MgZn_2$) is supported by EDS peaks from location d (Fig. 9(c)). Fig. 9(a,b) shows some $MgZn_2$ particles encircled with magnesium grains. The presence of both $MgZn_2$ and magnesium in this area of the stirred zone is in agreement with the formation of eutectic structure.

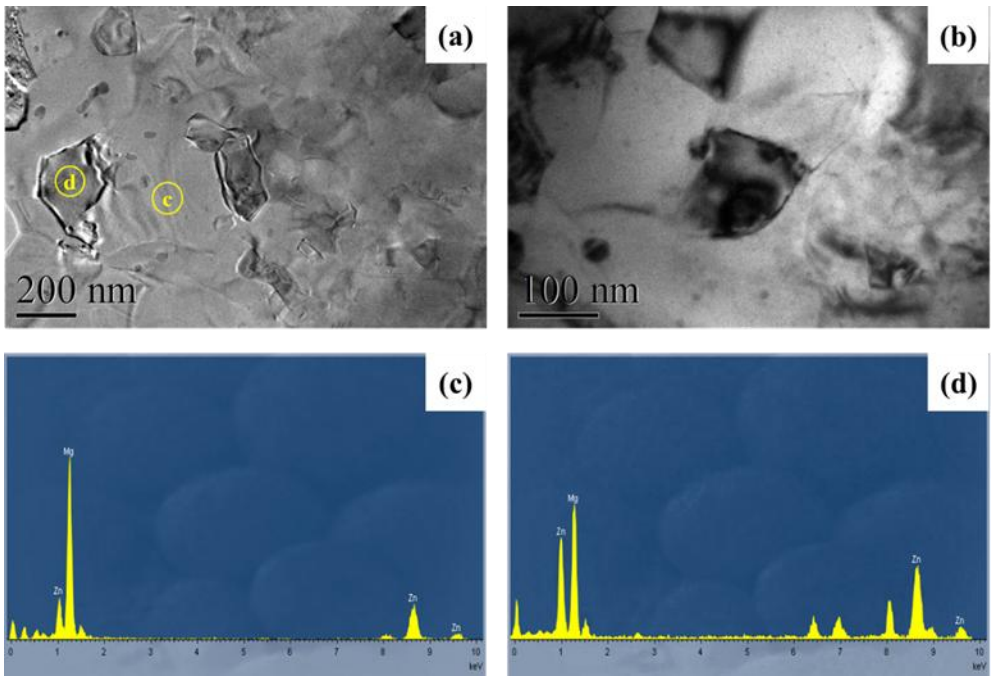

Fig. 9. TEM images and EDS analysis in stirred zone of the weld made at 600 rpm-35 mm/min: (a,b) bright-field images showing $MgZn_2$ phase and Zn-rich area in Mg matrix, (c,d) EDS peaks of points C and D denoted in Fig. 9(a).

3.3. Mechanical properties

3.3.1. Tensile properties

The tensile strength and elongation percentage of different Al-Mg butt welds with and without Zn interlayer, as a function of rotational and traveling speed, are shown in Fig. 10. Zn interlayer addition has obviously increased the tensile strength and elongation of the sound joints.

The main reasons for the lowest UTS and elongation in samples 1 and 2 are the incomplete intermixing of materials and the presence of tunnel and cavities, which decrease the effective working area and promote stress concentration, as shown in Figs. 3(a,b). The cross sectional area associated with the presence of void has been decreased in these samples. In addition, there are sharp edges inside the void, providing stress concentration condition and reducing both strength and elongation [41].

The heat input increased by increasing the rotational speed to 600 rpm in samples 3 and 4. This caused the improvement of the intermixing of Mg and Al alloys, removal of the microstructural defects and sufficient melting amount of the Zn interlayer. The latter in turns encourages the formation of the Mg-Zn IMCs to substitute the Al-Mg IMCs in the stirred zone. A small degree of deformation takes place prior to fracture when the brittle intermetallic is small. An ideal compound is one with lower hardness, which is more ductile than the Al-Mg IMCs, given the connection between the brittleness of a compound and its hardness [31]. Furthermore, Mg-Zn IMCs in the banded structure zone are in the form of eutectic structure and crack formation and propagation are harder compared with the formation of thick Al-Mg IMCs layers in this zone. Thus, sample 6, which was welded at 600 rpm and 35 mm/min speeds, showed the best UTS and elongation values.

As observed before in samples 5 and 6, a mixture of Mg-Zn eutectic phase and Al-Mg IMC layers form in the BS zone near the Mg interface due to the high temperature exposition, affecting therefore the mechanical properties of the joints. However, formation of more catastrophic Al-Mg IMC layers in addition to the presence of cavity defects in sample 5 have given lower mechanical properties than in sample 6.

The highest strength and elongation cannot be assured by any of the high rotational and low traveling speeds (maximum heat input) or low rotational and high traveling speeds (minimum heat input) in Zn added samples (Fig. 10). The efficiency of Zn interlayer addition and microstructural defects are affected by the low and high heat generation in FSW process.

Under low heat input conditions (lower rotational and higher traveling speed), a smaller amount of Zn interlayer melts and diffusion of Zn atoms to the base materials is more difficult. Therefore, there are not sufficient Zn amount in the stir zone. Zn is an alternative in Al-Mg reactions and during welding, in which it reacts with Al, Mg or both base metals. Although larger amounts of Zn interlayer melt and atoms can diffuse more easily under high heat input conditions (higher rotational and lower traveling speed), more of the melted Zn is squeezed out under the action of FSW tool and more Al and Mg are intermixed due to the softening of materials, which can increase the possibility of forming Al-Mg IMC layers in the stirred and BS zones. Accordingly, due to the appropriate heat input in sample 4, a uniform eutectic structure of α (Mg) and Mg-Zn IMCs without the existence of any Al-Mg IMC layers is formed in the area near the Mg interface. Hence, sample 6 shows the best UTS and elongation values. This sample shows considerable improvement over sample 7, which has been welded under the same conditions without the addition of Zn interlayer.

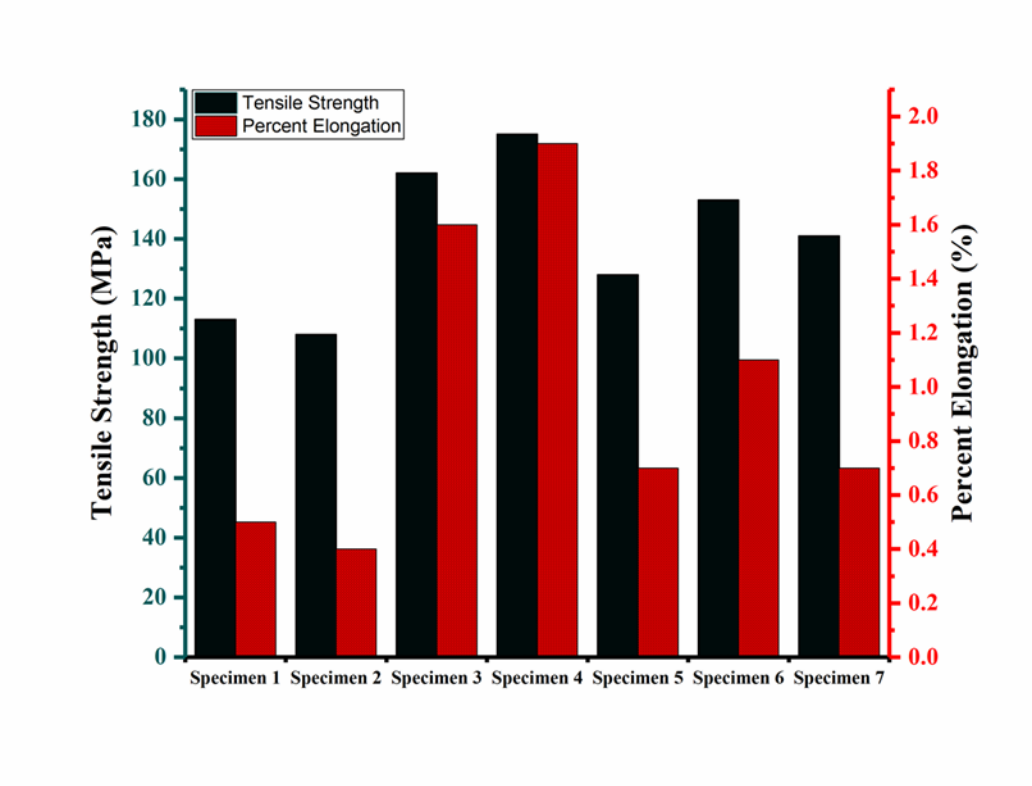

Fig. 10. UTS values and elongation percent of the welds.

3.3.2. Fractography

The fracture surfaces are given in Fig. 11. Figs. 11(a-f) and Fig. 11(g) show the fracture surfaces of Al/Mg joints with and without Zn interlayer, respectively. All the samples have been fractured along the banded structure zone adjacent to the AS. The sample without Zn interlayer shows a completely brittle fracture with coarse cleavage facets and vertical crack propagation.

For samples 1 and 2 (welded at 550 rpm), fracture with coarse cleavage facets also occurs. However, the size of facets are smaller and the surface texture is finer than Zn free sample and very shallow dimples can be observed on the fractured surface of these samples. This brittle behavior can be due to the presence of microstructural defects (Figs. 3(a,b)). In sample 1, the formation of Al-Mg IMC layers in BS zone (Fig. 5(a)) could be another reason. The fracture surfaces of samples 5 and 6 (welded at 650 rpm) have a finer texture and relatively deeper dimples compared with samples welded at low heat input (samples 1, 2). However, the fracture surfaces are smooth and do not show voids as expected in the case of plastic deformation. Formation of Al-Mg IMCs next to the eutectic structure of α (Mg) + Mg-Zn in BS zone of these samples can be the main reason for this behavior.

In samples 3 and 4, welded at moderate heat input (rotational speed of 600 rpm), a sort of serrate and fine texture of fracture surface are observed. In addition, dimples are more numerous and deeper compared with previous samples. The presence of such characteristics indicates noticeable ductility before fracture and switching the ailure behavior from brittle to the ductile mode. These features are more prominent in sample 4.

Ductility results are in full agreement with fracture micrographs. The smooth and coarse cleavage facets in fracture surface are responsible for the low elongations in samples 1, 2, 5 and 7 (Figs. 11(a,b,e,g)). Dorbane et al. have reported similar low elongation for defective Al/Mg joints [23].

Figs. 11(c,f) show moderate elongation for samples 3 and 6 is in accordance with the presence of fine texture and shallow dimples in the fracture surface. This is consistent with Lu et al. [33] and Gao et al. [34] reports.

The highest elongation and corresponding fractography display deep equiaxed dimples and uneven fracture surface as shown in sample 4, suggesting a strong ductile fracture component (Fig. 11(d)).

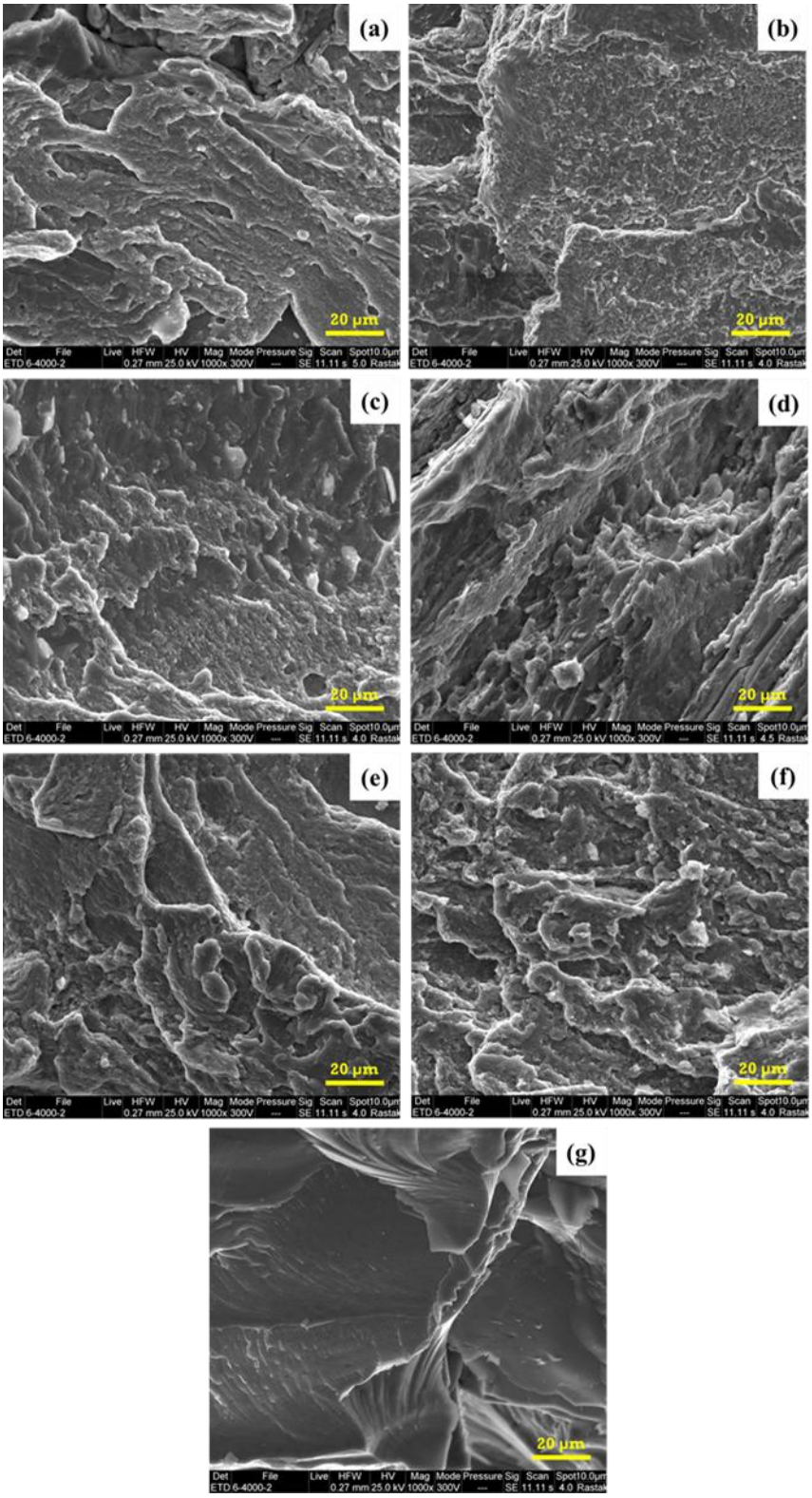

Fig. 11. Micro fractographs of sample: (a) nomber 1, (b) nomber 2, (c) nomber 3, (d) nomber 4, (e) nomber 5, (f) nomber 6 and (g) nomber 7.

Fig. 12 shows the XRD analysis on the Mg side of the fracture surface for the sample welded at 600 rpm and 35 mm/min. The XRD image shows $MgZn_2$ IMC diffraction peaks, Mg strong peaks and Al and Zn small peaks. This is in accordance with the EDS analysis of eutectic structure close to the Mg alloy in this sample. Nevertheless, $MgZn_2$ peaks are weaker than those of Mg because of the small surface area of the former particles in comparison with the Mg region on the fracture surface of Mg. This indicates that the fracture has occurred from $MgZn_2$ IMCs and continued through the eutectic structure. It must be pointed out that Mg-Al IMCs were not found in the XRD pattern of the fracture surface, which suggests the prevention of Al-Mg IMC formation by proper Zn interlayer.

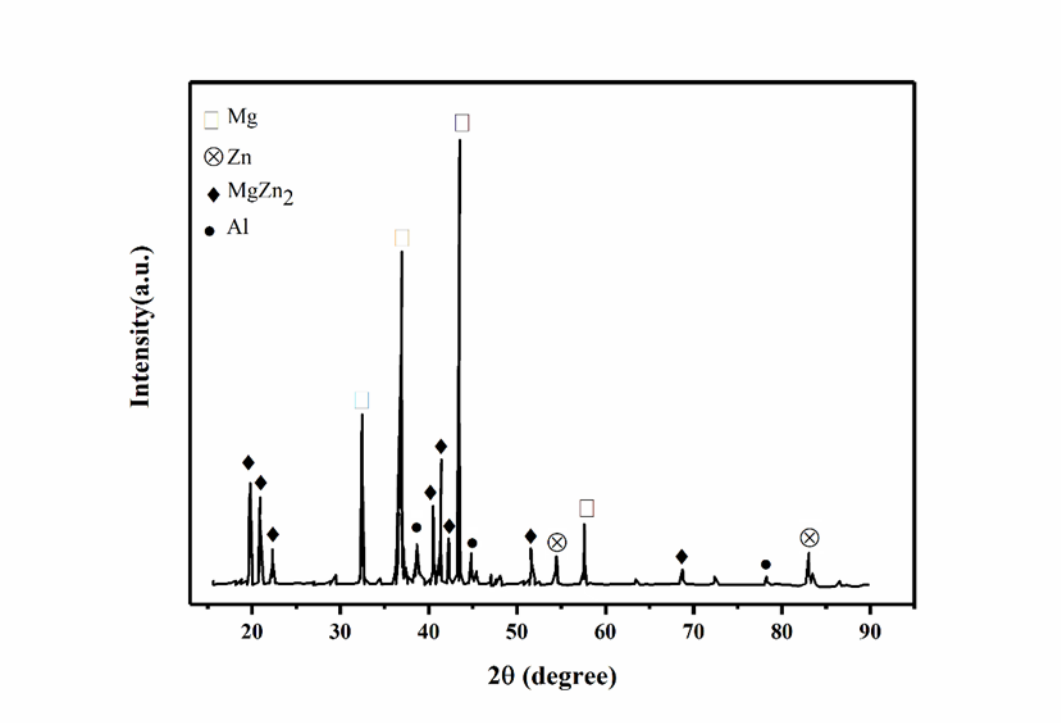

Fig. 12. XRD spectrum of fracture surface on Mg side for specimen no. 4.

3.3.3. Hardness

Fig. 13 shows the microhardness profile across the mid thickness of samples 4 and 5 (as a case study of two typical behavior of Zn added samples) in comparison with microhardness profile of sample 7 (non-reinforced sample). Hardness remarkably increases in all the welded samples in the stirred zone as a result of the so-called continuos recrystallization during FSW process and thus the presence of very small grains in this area [42]. The presence of IMCs is responsible for fluctuations in the points with high hardness. Next to the Mg base metal, the microhardness reaches the highest value, which is the same for Zn added and free joints. The average microhardness values and fluctuations in the stirred zone of sample 4 are lower than those of sample 5. This is in agreement with microstructural observations for sample 5, about the reformation of Al-Mg IMCs at high temperatures, especially near the Mg interface on advancing side (Fig. 5 (e)).

Microhardness is decreased by the addition of Zn interlayer, as shown by the comparison of Zn added (no. 4, 5) and free samples (no. 7). IMC formation was not avoided by the Zn added Al-Mg joints. However, there was a conversion from Al-Mg to Mg-Zn IMCs due to the addition of Zn interlayer, which reduced the value of microhardness peak.

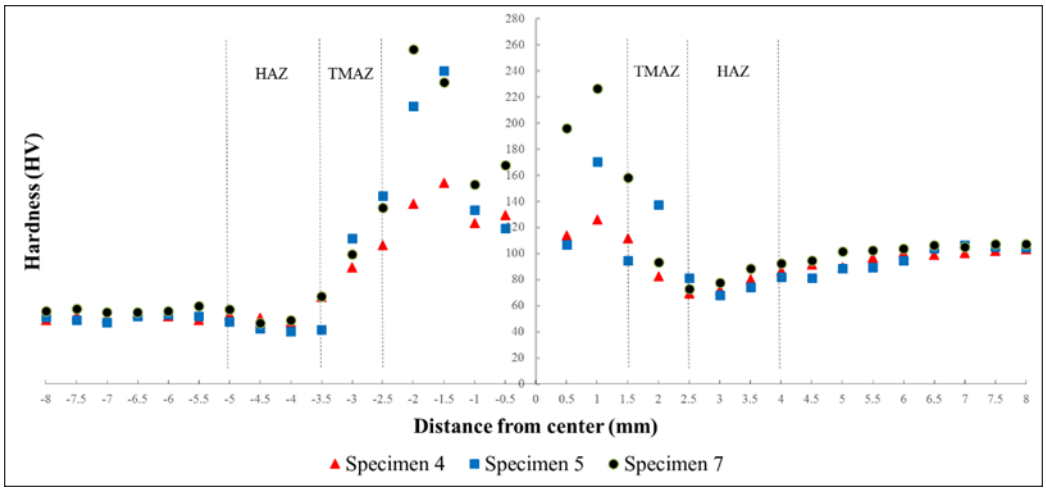

Fig. 13. Microhardness behavior across the centerline of sample 4, 5 and 7.

4. Conclusions

In this work, butt joints of AZ31 Mg and 6061 Al alloys were friction stir welded with the addition of Zn interlayer in a combination of two travel and three rotation speeds. The following findings were obtained by the evaluation of the microstructure and mechanical characteristics of the welds:

- The optimal travel and rotation speeds were 35 mm/min and 600 rpm, respectively, based on the microstructural observations and mechanical tests of the welded samples. The UTS of this sample improved from 141 to 175 MPa compared with the Zn free sample at the same process parameters and an improvement in the elongation from 0.7 to 1.9 was observed.

- The stirred zone of the Zn added joints contained Mg and Mg-Zn eutectic structures, Al-Mg-Zn IMC, and solid solutions whereas there were brittle $Mg_{17}Al_{12}$ and Mg_2Al_3 IMCs in the Zn-free joints. Application of low or high rotational speed led to the lack of Zn element and the presence of Al-Mg IMCs.

- All the samples have fractured along the region adjacent to the Mg alloy on the advancing side of the stirred zone. In the cases of formation layer shape Al-Mg IMCs in this region, the brittle fracture occurs while the fracture surface shows prominent ductile features if α (Mg) + $MgZn_2$ eutectic structure forms. Mg-Zn IMCs have less brittleness and are also in the form of eutectic structure in this region. Therefore, crack formation and propagation is more difficult in comparison with the existing layer shape Al-Mg IMCs.

- The average microhardness of the stirred zone was lower than that of the Zn free sample for the reinforced sample because of the substitution of Al-Mg IMCs with Mg-Zn and Al-Mg-Zn IMCs in the stirred zone of Zn added samples, which have lower hardness values. The absence of layer shape Al-Mg IMCs in the stirred zone and region near the Mg interface were confirmed by the low hardness fluctuations of sample welded at 35 mm/min and 600 rpm.

Acknowledgment

The authors appreciate the Polytechnic University of Catalonia and K.N. Toosi University of Technology for facilities provided for this work. In addition, special thanks should be given to Dr. Jessica Calvo and Dr. Jose Antonio Benito for their intellectual and practical support during this research.

References

[1] Ji SD, Meng XC, Liu JG, Zhang LG, Gao SS. Formation and mechanical properties of stationary shoulder friction stir welded 6005A-T6 aluminum alloy. Mater Des 2014;62:113–7.

[2] Ji S, Huang R, Meng X, Zhang L, Huang Y. Enhancing friction stir weldability of 6061-T6 Al and AZ31B Mg alloys assisted by external non-rotational shoulder. J Mater Eng Perform 2017;26:2359–67.

[3] Abdolahzadeh A, Omidvar H, Safarkhanian MA, Bahrami M. Studying microstructure and mechanical properties of SiC-incorporated AZ31 joints fabricated through FSW: the effects of rotational and traveling speeds. Int J Adv Manuf Technol 2014;75:1189–96.

[4] Abbasi M, Abdollahzadeh A, Omidvar H, Bagheri B, Rezaei M. Incorporation of SiC particles in FS welded zone of AZ31 Mg alloy to improve the mechanical properties and corrosion resistance. Int J Mater Res 2016;107:566–72.

[5] Venkateswaran P, Reynolds AP. Factors affecting the properties of Friction Stir Welds between aluminum and magnesium alloys. Mater Sci Eng A 2012;545:26–37.

[6] Chen YC, Nakata K. Friction stir lap joining aluminum and magnesium alloys. Scr Mater 2008;58:433–6.

[7] Mohammadi J, Behnamian Y, Mostafaei A, Izadi H, Saeid T, Kokabi AH, et al. Friction stir welding joint of dissimilar materials between AZ31B magnesium and 6061 aluminum alloys: Microstructure studies and mechanical characterizations. Mater Charact 2015;101:189–207.

[8] Lee C-Y, Lee W-B, Kim J-W, Choi D-H, Yeon Y-M, Jung S-B. Lap joint properties of FSWed dissimilar formed 5052 Al and 6061 Al alloys with different thickness. J Mater Sci 2008;43:3296–304.

[9] Rao HM, Ghaffari B, Yuan W, Jordon JB, Badarinarayan H. Effect of process parameters on microstructure and mechanical behaviors of friction stir linear welded aluminum to magnesium. Mater Sci Eng A 2016;651:27–36.

[10] Mofid MA, Abdollah-Zadeh A, Ghaini FM. The effect of water cooling during dissimilar friction stir welding of Al alloy to Mg alloy. Mater Des 2012;36:161–7.

[11] Abbasi M, Abdollahzadeh A, Bagheri B, Omidvar H. The Effect of SiC Particle Addition During FSW on Microstructure and Mechanical Properties of AZ31 Magnesium Alloy. J Mater Eng Perform 2015;24:5037–45.

[12] Abdollahzadeh A, Shokuhfar A, Omidvar H, Cabrera JM, Solonin A, Ostovari A, et al. Structural evaluation

and mechanical properties of AZ31/SiC nano-composite produced by friction stir welding process at various welding speeds. Proc Inst Mech Eng Part L J Mater Des Appl 2017:1464420717708485.

[13] Plaine AH, Gonzalez AR, Suhuddin UFH, Dos Santos JF, Alcântara NG. The optimization of friction spot welding process parameters in AA6181-T4 and Ti6Al4V dissimilar joints. Mater Des 2015;83:36–41.

[14] Sahu PK, Pal S, Pal SK, Jain R. Influence of plate position, tool offset and tool rotational speed on mechanical properties and microstructures of dissimilar Al/Cu friction stir welding joints. J Mater Process Technol 2016;235:55–67.

[15] Rafiei R, Moghaddam AO, Hatami MR, Khodabakhshi F, Abdolahzadeh A, Shokuhfar A. Microstructural characteristics and mechanical properties of the dissimilar friction-stir butt welds between an Al–Mg alloy and A316L stainless steel. Int J Adv Manuf Technol 2017;90:2785–801.

[16] Fallahi AA, Shokuhfar A, Moghaddam AO, Abdolahzadeh A. Analysis of SiC nano-powder effects on friction stir welding of dissimilar Al-Mg alloy to A316L stainless steel. J Manuf Process 2017;30:418–30.

[17] Aonuma M, Nakata K. Dissimilar metal joining of ZK60 magnesium alloy and titanium by friction stir welding. Mater Sci Eng B 2012;177:543–8.

[18] Rao HM, Yuan W, Badarinarayan H. Effect of process parameters on mechanical properties of friction stir spot welded magnesium to aluminum alloys. Mater Des 2015;66:235–45.

[19] Zhao Y, Lu Z, Yan K, Huang L. Microstructural characterizations and mechanical properties in underwater friction stir welding of aluminum and magnesium dissimilar alloys. Mater Des 2015;65:675–81.

[20] Buffa G, Baffari D, Di Caro A, Fratini L. Friction stir welding of dissimilar aluminium–magnesium joints: sheet mutual position effects. Sci Technol Weld Join 2015;20:271–9.

[21] Fu B, Qin G, Li F, Meng X, Zhang J, Wu C. Friction stir welding process of dissimilar metals of 6061-T6 aluminum alloy to AZ31B magnesium alloy. J Mater Process Technol 2015;218:38–47.

[22] Liang Z, Chen K, Wang X, Yao J, Yang Q, Zhang L, et al. Effect of tool offset and tool rotational speed on enhancing mechanical property of Al/Mg dissimilar FSW joints. Metall Mater Trans A 2013;44:3721–31.

[23] Dorbane A, Mansoor B, Ayoub G, Shunmugasamy VC, Imad A. Mechanical, microstructural and fracture properties of dissimilar welds produced by friction stir welding of AZ31B and Al6061. Mater Sci Eng A 2016;651:720–33.

[24] Firouzdor V, Kou S. Al-to-Mg friction stir welding: effect of material position, travel speed, and rotation speed. Metall Mater Trans A 2010;41:2914–35.

[25] Firouzdor V, Kou S. Formation of liquid and intermetallics in Al-to-Mg friction stir welding. Metall Mater Trans A 2010;41:3238–51.

[26] Dai X, Zhang H, Wang B, Ji A, Liu J, Feng J. Improving weld strength of arc-assisted ultrasonic seam welded Mg/Al joint with Sn interlayer. Mater Des 2016;98:262–71.

[27] Penner P, Liu L, Gerlich A, Zhou Y. Feasibility study of resistance spot welding of dissimilar Al/Mg combinations with Ni based interlayers. Sci Technol Weld Join 2013;18:541–50.

[28] Sun M, Niknejad ST, Zhang G, Lee MK, Wu L, Zhou Y. Microstructure and mechanical properties of resistance spot welded AZ31/AA5754 using a nickel interlayer. Mater Des 2015;87:905–13.

[29] Patel VK, Bhole SD, Chen DL. Improving weld strength of magnesium to aluminium dissimilar joints via tin interlayer during ultrasonic spot welding. Sci Technol Weld Join 2012;17:342–7.

[30] Wang Y, Luo G, Zhang J, Shen Q, Zhang L. Microstructure and mechanical properties of diffusion-bonded Mg–Al joints using silver film as interlayer. Mater Sci Eng A 2013;559:868–74.

[31] Shah LH, Gerlich A, Zhou Y. Design guideline for intermetallic compound mitigation in Al-Mg dissimilar welding through addition of interlayer. Int J Adv Manuf Technol 2018;94:2667–78.

[32] Liu LM, Zhao LM, Xu RZ. Effect of interlayer composition on the microstructure and strength of diffusion bonded Mg/Al joint. Mater Des 2009;30:4548–51.

[33] Liu F, Zhang Z, Liu L. Microstructure evolution of Al/Mg butt joints welded by gas tungsten arc with Zn filler metal. Mater Charact 2012;69:84–9.

[34] Gao Q, Wang K. Influence of Zn interlayer on interfacial microstructure and mechanical properties of TIG lap-welded Mg/Al joints. J Mater Eng Perform 2016;25:756–63.

[35] Dai X, Zhang H, Zhang H, Liu J, Feng J. Arc assisted ultrasonic seam welding of Mg/Al joints with Zn interlayer. Mater Sci Technol 2016;32:164–72.

[36] Mishra RS, De PS, Kumar N. Friction stir welding and processing: science and engineering. Springer; 2014.

[37] Shi H, Chen K, Liang Z, Dong F, Yu T, Dong X, et al. Intermetallic compounds in the banded structure and their effect on mechanical properties of Al/Mg dissimilar friction stir welding joints. J Mater Sci Technol 2017;33:359–66.

[38] Lohwasser D, Chen Z. Friction stir welding: From basics to applications. Elsevier; 2009.

[39] Zhang Y, Luo Z, Li Y, Liu Z, Huang Z. Microstructure characterization and tensile properties of Mg/Al dissimilar joints manufactured by thermo-compensated resistance spot welding with Zn interlayer. Mater Des 2015;75:166–73.

[40] Villars P, Prince A, Okamoto H. Handbook of ternary alloy phase diagrams. Asm Intl; 1995.

[41] Hertzberg RW. Deformation and fracture mechanics of engineering materials 1989.

[42] Mishra RS, Ma ZY. Friction stir welding and processing. Mater Sci Eng R Reports 2005;50:1–78.